Optical Materials 101 (2020) 109738

Contents lists available at ScienceDirect

Optical Materials

journal homepage: http://www.elsevier.com/locate/optmat

Investigating the performance of formamidinium tin-based perovskite solar cell by SCAPS device simulation

S. Abdelaziz [a], A. Zekry [a], A. Shaker [b,*], M. Abouelatta [a]

[a] Electronics and Communications Dept, Faculty of Engineering, Ain Shams University, Cairo, Egypt
[b] Engineering Physics and Mathematics Dept, Faculty of Engineering, Ain Shams University, Cairo, Egypt

ARTICLE INFO

Keywords:
Tin-based perovskite
Hole transport layer (HTL)
Electron transport layer (ETL)
SCAPS
Power conversion efficiency (PCE)

ABSTRACT

Tin-based perovskite is a famous competitor to toxic lead-based perovskite solar cells. Although lead-free perovskite ($CH_3NH_3SnI_3$) material attracts the attention because of its wider absorption, it suffers from temperature instability. Formamidinium tin iodide ($HC(NH_2)_2SnI_3$– $FASnI_3$) absorber has more temperature stability than $CH_3NH_3SnI_3$ with wider band gap (1.41 eV). In this work, a device simulation of $FASnI_3$- based solar cells is performed by using SCAPS. Absorber parameters such as thickness, doping concentration and defect density are varied to inspect their impact on device performance. The effect of changing conduction band offset (CBO) and valence band offset (VBO), doping concentration and thickness of electron transport layer (ETL) and hole transport layer (HTL) are also studied. Further, various HTL and ETL candidates are investigated such as CuI, Cu_2O, NiO, ZnO and ZnSe. To enhance the cell power efficiency, optimization of the device design key parameters is performed. The initial structure is based on an experimental work having a record of 1.75% efficiency. The final performance parameters of the intended solar cell after enhancing them by the presented parametric study are found to be: a short-circuit current density (J_{sc}) of 22.65 mA/cm^2, open-circuit voltage (V_{oc}) of 0.92 V, fill factor (*FF*) of 67.74% and power conversion efficiency (*PCE*) of 14.03%.

1. Introduction

Recently, halide perovskite has a promising performance in solar cell technology. Despite high reported power conversion efficiency (*PCE*) of lead-based perovskite which exceeds 20% [1], instability and toxicity of lead give a cause for concern. Two approaches are exhibited to decrease toxicity of metal halide perovskite. The first approach is done by mixing lead with other metals which have lower toxicity such as tin-lead alloyed perovskite ($CH_3NH_3Sn_xPb_{1-x}$) [2,3]. The second technique is done by completely replace lead with analogous metals. As a candidate of lead, the innocuous Tin is considered the most suitable material because both are in the same group in the periodic table.

Although tin-based perovskite is demonstrated as adequate lead-free absorber, tin-based devices suffer from the instability of Sn^{+2} which is easily oxidized into Sn^{+4} when uncovered to air. Consequently, high doped hole concentration is formed in the perovskite film which makes carrier recombination more significant [4,5]. To overcome this problem, SnF_2 is added to the system in order to decline oxidation of Sn^{+2} and hence a denser and more stable perovskite film is resulted [6,7].

Further, despite hopeful absorbing properties of $CH_3NH_3SnI_3$ and $CsSnI_3$ [7,8], they suffer from main temperature instability issue. This instability issue is related to the organic cation employed in perovskite. It has been observed that using formamidinium $HC(NH_2)_2$ in place of CH_3NH_3 introduces more solid perovskite structure and hence more stable materials [9]. Formamidinium tin iodide absorber ($HC(NH_2)_2SnI_3$– $FASnI_3$) has an energy band gap of 1.41 eV and its absorption starts at 880 nm.

Recently, many approaches have been presented to improve the performance of $FASnI_3$ based devices. Employing a SnF_2-pyrazine complex or using inverted structure is leading to increase the *PCE* to 4.8% and 6.22% respectively [10,11]. Also, open-circuit voltage can be enhanced by using cascaded (TiO_2–ZnS) electron transport layer [12]. Despite the progress in improving performance of $FASnI_3$ devices, the *PCE* is very limited which makes the simulation of these devices very vital to understand the relationship between device parameters and cell performance. In this work, we investigate the simulation of formamidinium tin iodide ($HC(NH_2)_2SnI_3$– $FASnI_3$) device for the first time.

The simulations are performed by utilizing the solar cell capacitance simulator SCAPS (ver.3.3.02) under AM1.5G illumination. SCAPS is a

* Corresponding author.
E-mail address: ahmed.shaker@eng.asu.edu.eg (A. Shaker).

https://doi.org/10.1016/j.optmat.2020.109738
Received 2 August 2019; Received in revised form 24 January 2020; Accepted 4 February 2020

one-dimensional opto-electrical simulator that is applied to structures of many semiconductor layers. Its working principle is based on solving continuity and Poisson equations. The number of layers can be increased up to seven layers and the simulation can be done under both light and dark conditions. It also allows defect levels in bulk and at interfaces. It can be applied to crystalline solar cells as well as amorphous cells [13–16].

2. Simulation parameters

The device architecture and energy band diagram of the solar cell under investigation are shown in Fig. 1. The cell is composed of glass substrate/FTO/TiO_2 (electron transport layer (ETL))/$FASnI_3$ (perovskite layer)/Spiro-OMeTAD (hole transport layer (HTL))/Au (metal back contact) as shown in Fig. 1(a). The energy band gaps and affinities of the main layers are shown in Fig. 1(b), while the energy band diagram is illustrated in Fig. 1(c).

Table 1 includes the basic parameters of ETL, HTL and FTO which are based on some previously published literature [17–22]. Other parameters are assumed to be the same for all layers such as thermal velocities of both electrons and holes which are set to 10^7 cm/s. Parameters of $FASnI_3$ material are set according to some published works [11,23–26]. As mentioned in Ref. [11], the charge carrier density of $FASnI_3$ is p-type and does not depend on the SnF_2 concentration; but, only on the presence of SnF_2 and it is in the range of $(1 \times 10^{17}–2 \times 10^{17})$ cm^{-3}. For best calibrations, $FASnI_3$ device is assumed to have initial hole carrier density of 7.0×10^{16} cm^{-3}. The Initial defect density in the absorber layer is assumed to be 2.0×10^{15} cm^{-3} to get a carrier lifetime of 2.5 ns This value is matched with the theoretical literature range (1 ns- 4 ns) [27,28] in $FASnI_3$ devices treated by SnF_2. The interface defects at ETL/absorber and absorber/HTM interfaces are considered single and neutral. Table 2 summarizes the defect density inside the absorber and at interfaces. The work function of FTO and back metal are set to 4 and 5.1 eV, respectively. A series resistance is assumed to be 5.4 Ω cm^2.

The initial cell technological and geometrical parameters are extracted from an experimental solar cell featuring the same materials [23]. Simulation results using these initial parameters, regarding the current density–voltage (*J-V*) characteristic, give the following cell performance parameters: short-circuit current density (J_{sc}) is 14.45 mA/cm^2, open-circuit voltage (V_{oc}) is 0.261 V, fill factor (*FF*) is 43.91% and power conversion efficiency (*PCE*) is 1.66%. Fig. 2 shows a comparison between simulation results and measurements. The *J-V* characteristic is shown in Fig. 2(a) while the quantum efficiency is illustrated in Fig. 2(b). In addition, a comparison between the main cell parameters is shown in Table 3. A good matching between measurements and our calibration is observed which is a proof of validation of our simulation.

Furthermore, in Fig. 3(a), the simulated dark (*J-V*) characteristic is compared to illumination one. The comparison verifies that the collection process of this perovskite solar cell is perfect since no intersection between the two curves. Based on the single diode model, the ideality factor *n*, the reverse saturation current J_o and series resistance R_s can be extracted by plotting the dark characteristic current in a log scale as shown in Fig. 3(b) [29]. Calculations depending on this concept give an ideality factor of 1.4, a reverse saturation current of 9.04 μA/cm^2 and series resistance of 5.5 Ω cm^2. It is noticed that while the ideality factor

Table 1
Basic parameters of each layer.

Parameters	FTO	TiO_2	$FASnI_3$	Spiro-OMeTAD
Thickness (nm)	500	30	350	200
Band gap (eV)	3.5	3.2 [17]	1.41 [23]	2.88
Electron affinity (eV)	4	4 [18]	3.52 [24]	2.05 [17]
Dielectric Permittivity	9	9 [19]	8.2 [25]	3 [21]
CB effective density of states (cm^{-3})	2.2×10^{18}	2.0×10^{18}	1.0×10^{18}	2.2×10^{18}
VB effective density of states (cm^{-3})	1.8×10^{19}	1.8×10^{19}	1.0×10^{18}	1.8×10^{19}
Electron mobility (cm^2/V.s)	20	20 [17]	22 [26]	2.0×10^{-4} [22]
Hole mobility (cm^2/V.s)	10	10 [17]	22 [26]	2.0×10^{-4} [22]
Shallow donor density N_D (cm^{-3})	2.0×10^{19}	9.0×10^{16}	–	–
Shallow Acceptor density N_A (cm^{-3})	–	–	7.0×10^{16}	2.0×10^{19} [17]
Defect density N_t (cm^{-3})	1.0×10^{15}	1.0×10^{15} [20]	2.0×10^{15}	1.0×10^{15}

Table 2
Defect density inside the absorber and at interfaces.

	ETL/absorber	absorber/HTM	$FASnI_3$
Defect type	Neutral	Neutral	Neutral
Capture cross section for electron and holes (cm^{-2})	1.0×10^{-15}	1.0×10^{-15}	2.0×10^{-14}
Energetic distribution	Single	Single	Gaussian
Energy level with respect to E_v	0.6	0.6	0.65
Characteristic energy (eV)	–	–	0.1
Total density (cm^{-3})	1.0×10^{16}	1.0×10^{16}	2.0×10^{15}

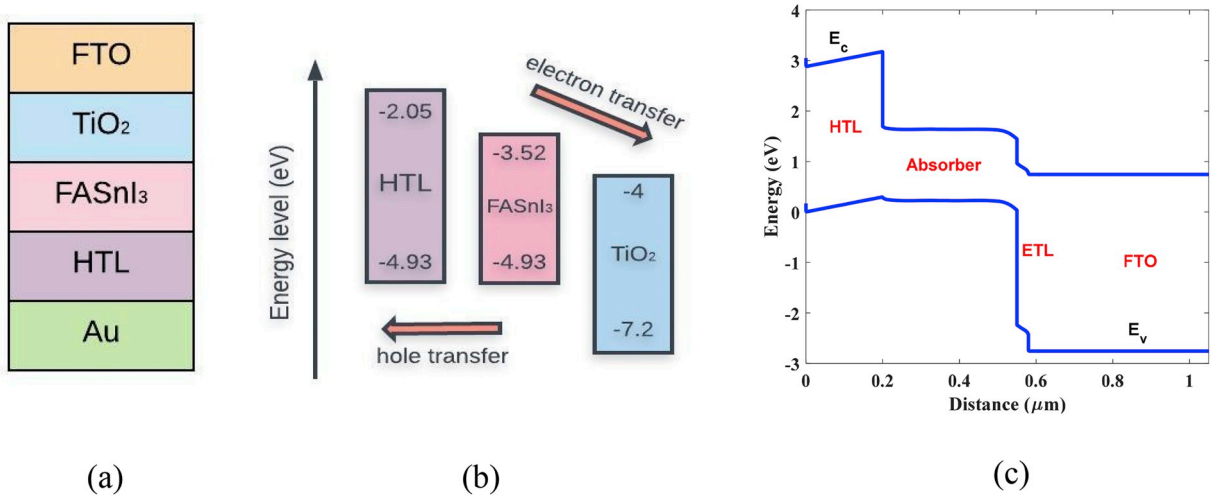

Fig. 1. Initial solar cell structure: (a) basic layers, (b) energy band diagram before contact and (c) energy band diagram after contact.

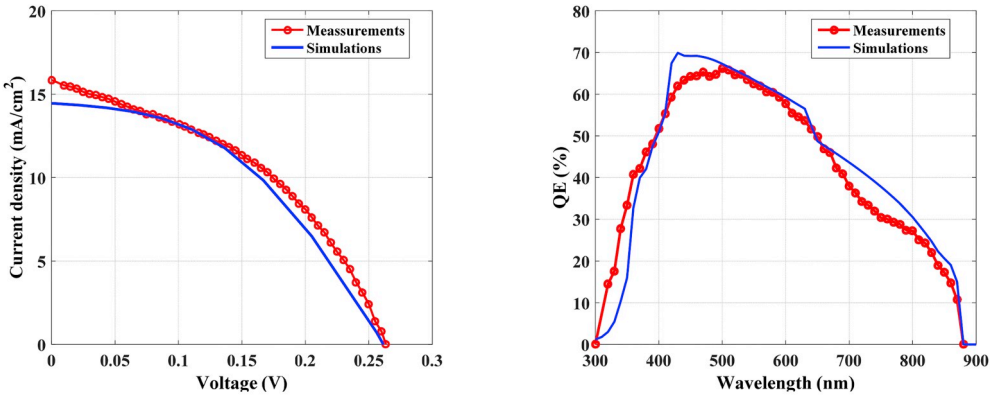

Fig. 2. Simulation versus measurements (a) current density–voltage characteristic (b) EQE.

Table 3
Simulated cell parameters versus measurements reported in literature.

	Measurement [23]	Simulation
J_{sc} (mA/cm^2)	15.85	14.45
V_{oc} (V)	0.264	0.261
FF (%)	42	43.91
PCE (%)	1.75	1.66

is ordinary, the reverse saturation current is too large. This could be the main cause for the too low conversion efficiency of such cells. Additionally, Fig. 3(b) demonstrates the local ideality factor. In such devices high ideality factor is obtained due to high carrier recombination processes in the bulk and surface regions [30].

In the next section, analyses are performed to inspect the influence of the device key factors on cell performance. These analyses include changing absorber parameters, defect density, and some HTL and ETL properties. Also, various HTL and ETL candidates are investigated. Optimization is performed for each parameter to get the maximum possible *PCE*.

3. Results and discussion

3.1. Effect of changing defect density (N_t) and absorber thickness

Trap-assisted Shockley–Read–Hall (SRH) recombination is dominant in $FASnI_3$ devices due to large defect density (N_t) caused by the poor film quality [31]. In such type of recombination, electrons in the conduction band or holes in valence band recombine through trap states [32]. SRH recombination can be expressed as in Equations (1) and (2) [33], where τ is the carrier lifetime and N_t and E_t are defect concentration and defect energy level, respectively. σ and V_{th} represent carriers capture cross section and thermal velocity, respectively.

$$R_{SRH} = \frac{np - n_i^2}{\tau\left(p + n + 2n_i \cosh\left(\frac{E_i - E_t}{KT}\right)\right)} \quad (1)$$

$$\tau = \frac{1}{\sigma \times N_t \times v_{th}} \quad (2)$$

The carrier diffusion length (L) in absorber layer can be calculated using Equation (3), where D is diffusion coefficient and D is given by the formula $D = \frac{KT}{q}\mu$.

$$L = \sqrt{D \times \tau} \quad (3)$$

As Equations (1)–(3) indicate, if defect density decreases, carrier lifetime increases and, hence, longer diffusion length and less recombination are observed. These are the main factors to improve cell performance. As shown in Fig. 4, decreasing N_t leads to less recombination rate inside the perovskite (Fig. 4(a)) and better (*J-V*) characteristics (Fig. 4(b)).

Moreover, Table 4 indicates the variation in diffusion length according to variation in defect density (N_t). Using the values given in the table, Fig. 5 illustrates the dependence of the *PCE* according to the

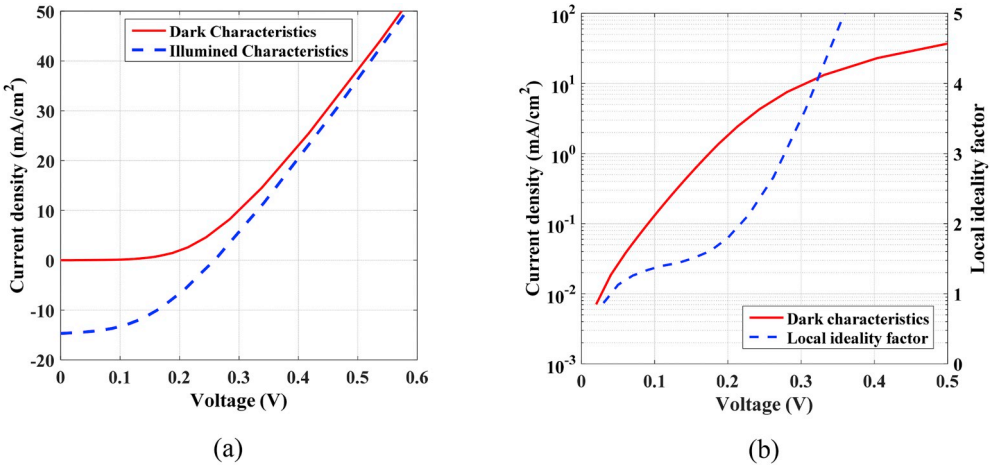

Fig. 3. (a) Dark versus illumination characteristics (b) Dark characteristic and local ideality factor.

variation of the absorber thickness for different diffusion lengths. It can be inferred, from the figure, that by lowering N_t (increasing L as a consequence), absorber thickness can be increased as much as diffusion length, and hence more absorption and higher PCE is obtained. Since there is no significant change in (*J-V*) characteristics when N_t changes from 10^{14} cm^{-3} to 10^{15} cm^{-3}, the optimum value of N_t is set to 10^{15} cm^{-3}. This trap density value gives a diffusion length $L = 0.53$ μm. According to this criterion, the *PCE* can reach as high as 2.2% at an absorber thickness of about 2 μm. The optimum value of the absorber thickness is taken as 530 nm since the diffusion length at the chosen N_t (10^{15} cm^{-3}) is 530 nm.

3.2. Effect of changing absorber doping

Tin-based perovskite suffer from high background carrier density which results from oxidation of Sn^{+2} in air. As the doping of absorber layer increases, more carriers can contribute in reverse saturation current causing its rise. Consequently, the open circuit voltage (V_{oc}) declines as Equation (4) expresses,

$$V_{oc} = n\, V_T \ln\left(1 + \frac{I_G}{I_0}\right) \tag{4}$$

where I_0 is the dark saturation current, n is the diode ideality factor, I_G is the light-generated current and V_T is the thermal voltage. From another point of view, when doping concentration increases, the electric field at the perovskite interface increases and the separation process will be enhanced. However, increasing recombination according to this increasing field will affect badly the performance. The influence of raising doping concentration on recombination inside perovskite is obvious in Fig. 6.

As indicated in Fig. 7, the open circuit voltage (V_{oc}) and power efficiency (*PCE*) reach a maximum value of 0.46 V and 4.59% at doping concentration of 10^{14} cm^{-3}, respectively. Since decreasing doping concentration is not a practical process, the optimum value of doping concentration (N_A) is set to 10^{15} cm^{-3} not 10^{14} cm^{-3}.

3.3. Effect of changing ETL and HTL parameters

Choosing HTL and ETL parameters are very critical in designing efficient solar cells [34]. Reducing charge recombination at the interfaces between absorber and ETL/HTL is significant to allow efficient carrier extraction. To achieve that, the conduction band offset (CBO) and valence band offset (VBO) should be carefully optimized. The sign of CBO and VBO can be positive or negative depending on the barrier height of photo-generated carriers as indicated in Equations (5) and (6).

$$\mathrm{CBO} = (\chi_{\mathrm{per}} - \chi_{\mathrm{ETL}}) \tag{5}$$

Table 4
Variation in diffusion length according to variation in Defect density (N_t).

N_t (cm^{-3})	10^{17}	10^{16}	2×10^{15}	10^{15}	10^{14}
L (μm)	0.053	0.17	0.38	0.53	1.7

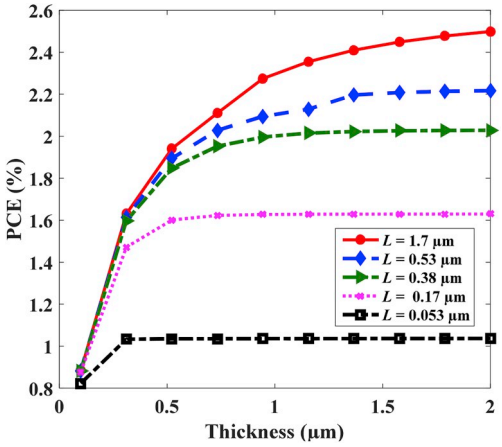

Fig. 5. Variation of power efficiency with absorber thickness at different diffusion length.

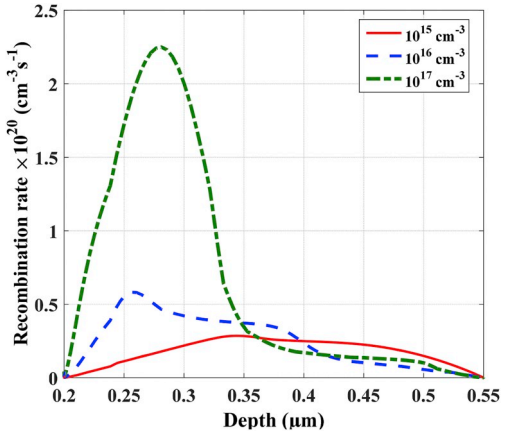

Fig. 6. Impact of changing background doping concentration (N_A) of absorber layer on recombination rates along the perovskite.

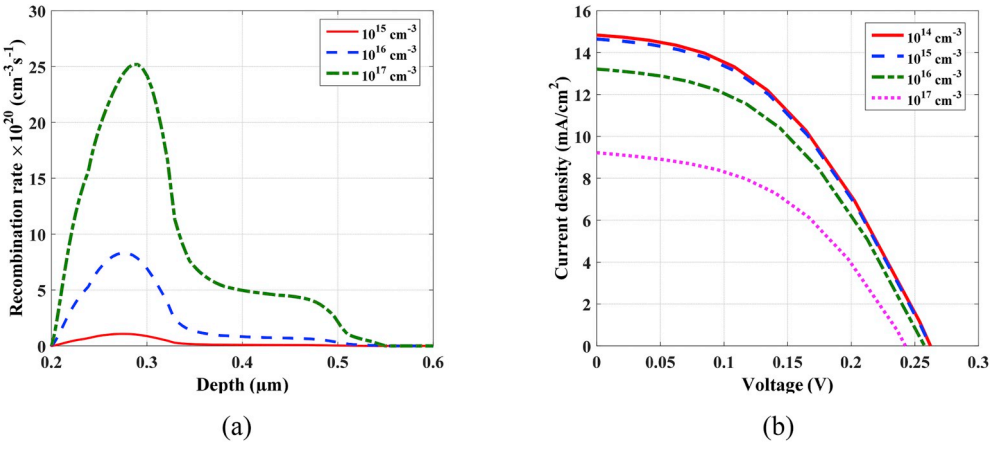

Fig. 4. Effect of changing absorber defect density (N_t) on (a) Recombination rate inside perovskite (b) current density-voltage curves.

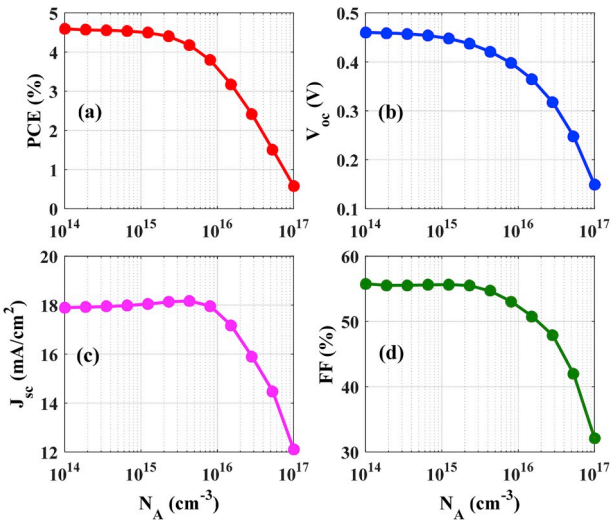

Fig. 7. Effect of changing doping concentration (N_A) of absorber layer on cell parameters.

$$\mathrm{VBO} = \left(\chi_{\mathrm{HTL}} - \chi_{\mathrm{per}} + E_{g\,\mathrm{HTL}} - E_{g\,\mathrm{per}}\right) \tag{6}$$

Where χ_{per}, χ_{ETL} and χ_{HTL} are the affinity of perovskite, ETL and HTL, respectively. $E_{g\,\mathrm{per}}$ and $E_{g\,\mathrm{HTL}}$ are the band gap of perovskite and HTL, respectively.

We study here the effect of changing CBO and VBO by changing both of ETL and HTL affinity. The simulated ETL affinity is changed in the range (3.2 eV–4.2 eV) and HTL affinity is changed in the range (1.95 eV–2.35 eV). Positive CBO/VBO lower up to 0.3 eV is very suitable to obtain lower recombination and larger open circuit voltage. While negative CBO/VBO results in more electron/holes accumulation at the interfaces and hence critical recombination and low charge output are obtained [35]. It can be inferred from Fig. 8(a) and (b) that the power efficiency reaches up to about 2.5% and 1.85% by increasing CBO and VBO to 0.3 eV, respectively. The optimum value of ETL and HTL affinity are taken as 3.5 eV and 2.15 eV respectively.

In addition to the affinity of ETL and HTL, also their conductivity plays a main rule in cell design. From the conductivity perspective, it should be high to reduce the ohmic losses of the cell. Controlling doping concentration of both ETL and HTL can be achieved by controlling the dopants types [36,37]. In our simulations here, the doping concentration of ETL and HTL are varied from 10^{16} cm^{-3} to 10^{20} cm^{-3} to study its influence on the performance. As noticed from Fig. 9, further improvement of *PCE* can be observed when ETL acceptor concentration (Fig. 9(a)) and HTL donor concentration (Fig. 9(b)) is raised. As it can be depicted from Fig. 9(a), the *PCE* remains nearly constant up to an ETL doping concentration of 1×10^{16} cm^{-3}. As the doping concentration exceeds 1×10^{16} cm^{-3}, the *PCE* increases rapidly up to about 6% at a concentration of 1×10^{20} cm^{-3}. In addition, the *PCE* increases slowly when the concentration of the HTL is up to 1×10^{16} cm^{-3}. Beyond this value of doping, the *PCE* increases rapidly as seen from Fig. 9(b). Taking into consideration the manufacturing hardness, the optimum value of ETL doping concentration is chosen to 1×10^{18} cm^{-3}. Also, the optimum value of HTL doping concentration is 5×10^{19} cm^{-3}. These values are chosen as it is difficult to obtain higher doping practically. In addition, high doping can generate deep Coulomb traps and, in turn, deteriorate the carrier mobility.

Our simulation also includes the effect of varying ETL/HTL thickness in the ranges of (10 nm–70 nm) and (0.05 μm–0.2 μm) for ETL and HTL, respectively as can be depicted from Fig. 10. It is obvious in Fig. 10(a) that *PCE* is raised to 3.5% with decreasing thickness of ETL to 0.01 μm, while it has a slight change when HTL thickness is halved as shown in Fig. 10(b). Reducing the thickness of HTL while keeping *PCE* unchanged can be useful in fabrication for reducing cost. We choose thickness of 20 nm and 50 nm as optimum values of ETL and HTL, respectively.

3.4. Other candidates of HTL and ETL

Using Spiro-MeOTAD and TiO_2 as HTL/ETL is very famous in normal $FASnI_3$ device. We use here (CuI, Cu_2O, NiO) and (ZnO, ZnSe) as Spiro-MeOTAD and TiO_2 alternatives, respectively. The main parameters of the suggested materials are shown in Table 5 [17,38,39]. Table 6 summarizes a comparison between device performances with different cell structures. As noticed in Table 6, using Cu_2O as an HTL candidate improves both J_{sc} and *PCE* as *PCE* value reaches 1.75%. On the other hand, using ZnO and ZnSe as an ETL alternative increases the open circuit voltage to 0.43 V and 0.37 V respectively. An enhancement in power efficiency and fill factor is also achieved when replacing ETL with these materials.

Finally, device optimizations according to results presented in section 3.1, 3.2 and 3.3 are performed and simulation is repeated with optimum value of each parameter. Fig. 11 shows the current density–voltage characteristics for the initial structure before optimization compared with each cycle of optimization.

Tables 7 and 8 summarize the optimum value for each absorber parameter and the device performance in each case, respectively. It is clear from Table 8 that optimization of doping concentration has the major effect in performance enhancement. After doping concentration optimization, open circuit voltage (V_{oc}) increases by about 75% (0.47) and power efficiency (*PCE*) is raised to a value almost three times larger than the initial value (which is 1.66% for the initial structure). The

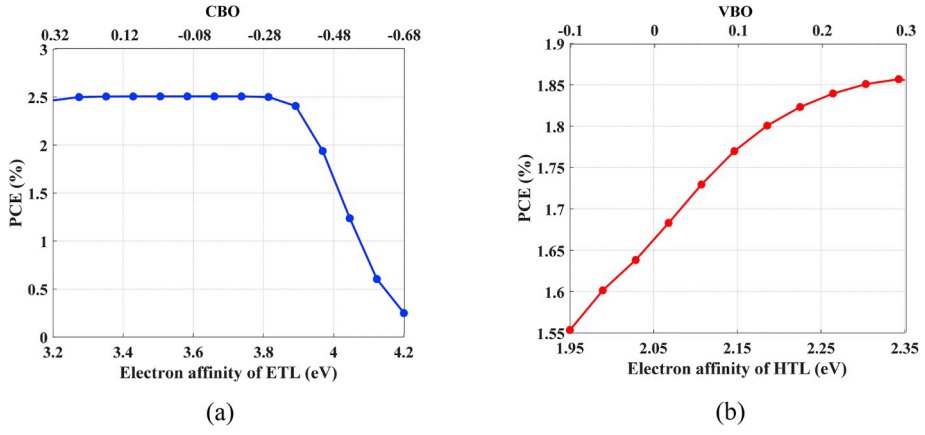

Fig. 8. Effect of electron affinity of (a) ETL and (b) HTL on *PCE*.

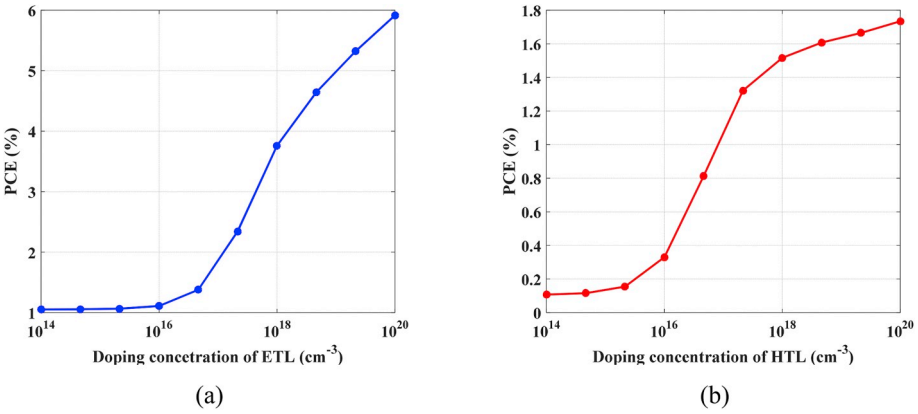

Fig. 9. Effect of changing doping concentration of (a) ETL and (b) HTL on *PCE*.

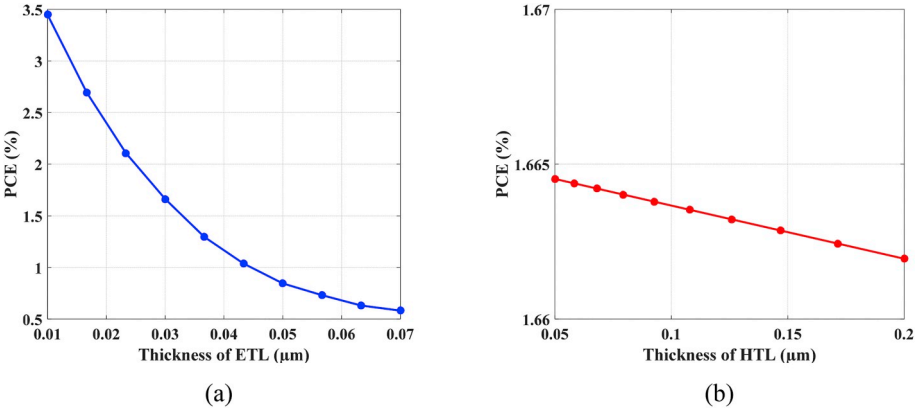

Fig. 10. Effect of thickness of (a) ETL and (b) HTL on *PCE*.

Table 5
Main parameters of selected materials for ETL and HTL.

Parameters	CuI	Cu_2O	NiO	ZnO	ZnSe
Band gap (eV)	2.98	2.1	3.6	3.3	2.81
Electron affinity (eV)	2.1	3.2	1.8	4	4.09
Doping (cm^{-3})	1.00×10^{18}	1.00×10^{18}	1.00×10^{18}	1.00×10^{18}	1.00×10^{18}
Electron/hole mobility (cm^2/Vs)	1.69×10^{-4}	3.4	0.2	100/25	400/110

Table 6
Comparison between device performance with different HTL/ETL alternatives.

Structure/cell parameters	J_{sc} (mA/cm^2)	V_{oc} (V)	*FF* (%)	PCE (%)
TiO_2/Spiro-MeOTAD	14.45	0.262	43.91	1.66
TiO_2/CuI	14.69	0.263	40.13	1.59
TiO_2/Cu_2O	15.57	0.265	43.07	1.78
TiO_2/NiO	15.86	0.266	38.06	1.60
ZnO/Spiro-MeOTAD	15.29	0.43	58.19	3.80
ZnSe/Spiro-MeOTAD	15.1	0.37	52.15	2.65

results obtained, after including all parameters optimization, are as following: J_{sc} of 22.65 mA/cm^2, V_{oc} of 0.92 V, *FF* of 67.74% and *PCE* of 14.03%.

4. Conclusion

Although many investigations are done on $FASnI_3$ solar cell structures, they suffer from poor performance especially low open circuit

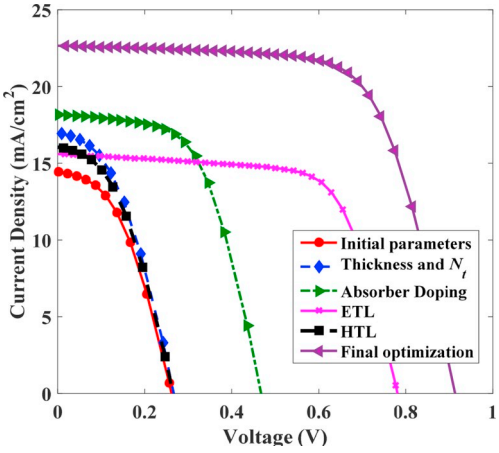

Fig. 11. Comparison of current density–voltage characteristic between initial, optimization of each parameter and final optimization.

Table 7
The optimum value of each parameter.

Optimized Parameters	Thickness (nm)	Doping Density (cm^{-3})	Defect Density (N_t) (cm^{-3})	Electron affinity (eV)
Absorber	530	1×10^{15}	10^{15}	–
ETL	20	1×10^{18}	–	3.5
HTL	50	5×10^{19}	–	2.15

Table 8
Device performance after optimization of each parameter.

	Initial	Absorber		ETL	HTL	Final Optimizations
		N_t and thickness	Doping Density			
J_{sc} (mA/cm^2)	14.45	16.97	18.18	15.6	16.05	22.65
V_{oc} (V)	0.262	0.268	0.47	0.78	0.266	0.915
FF (%)	43.91	41.78	57.27	68.37	42.68	67.74
PCE (%)	1.66	1.9	4.89	8.33	1.82	14.03

voltage and power efficiency. In this work, a device simulation of $FASnI_3$ has been done showing the impact of changing device parameters on cell performance. The simulation performed in this work is based on a systematic approach in which each device parameter is varied individually to see its impact on the device performance and to gain a physical insight of the reason behind its influence. Simulation results show that the self-oxidation of tin positive ions in such devices is the main issue of low performance as it leads to increasing background concentration and obtaining high recombination. Our results show that devices with lower doping concentration (N_A) have better performance. Another main issue in these devices is the film quality of perovskite. A denser and more uniform absorber film should decline defect density and enhance system behavior. In addition, our simulation results show that ETL and HTL parameters can greatly influence the cell performance. Simulations also prove that Spiro-MeOTAD and TiO_2 can be replaced by many suitable HTL materials that give a comparable performance. Enhancing absorber thickness, absorber defect density and doping density are performed. Also, ETL and HTL parameters like affinity, doping and thickness are varied to get maximum available efficiency. When including all parameters optimization, the final results are: J_{sc} of 22.65 mA/cm^2, V_{oc} of 0.92 V, *FF* of 76.74%. and *PCE* of 14.03%.

Author contributions

S. Abdelaziz: Collected the data, Contributed data or analysis tools, Performed the analysis, Performed the computer simulations, Wrote the paper.

A. Zekry: Conceived and designed the analysis, Contributed data or analysis tools, Wrote the paper.

A. Shaker: Conceived and designed the analysis, Contributed data or analysis tools, Wrote the paper.

M. Abouelatta: Conceived and designed the analysis, Contributed data or analysis tools, Wrote the paper.

Declaration of competing interest

The authors declare that they have no known competing financial interests or personal relationships that could have appeared to influence the work reported in this paper.

References

[1] L. Serrano-Lujan, N. Espinosa, T.T. Larsen-Olsen, J. Abad, A. Urbina, F.C. Krebs, Tin- and lead-based perovskite solar cells under scrutiny: an environmental perspective, Adv. Energy Mater. 5 (20) (2015), 1501119.

[2] Y. Ogomi, A. Morita, S. Tsukamoto, T. Saitho, N. Fujikawa, Q. Shen, et al., $CH_3NH_3Sn_xPb_{(1-x)}I_3$ perovskite solar cells covering up to 1060 nm, J. Phys. Chem. Lett. 5 (6) (2014) 1004–1011.

[3] F. Hao, C.C. Stoumpos, R.P.H. Chang, M.G. Kanatzidis, Anomalous band gap behavior in mixed Sn and Pb perovskites enables broadening of absorption spectrum in solar cells, J. Am. Chem. Soc. 136 (22) (2014) 8094–8099.

[4] N.K. Noel, S.D. Stranks, A. Abate, C. Wehrenfennig, S. Guarnera, A.-A. Haghighirad, et al., Lead-free organic–inorganic tin halide perovskites for photovoltaic applications, Energy Environ. Sci. 7 (9) (2014) 3061–3068.

[5] Shuyan Shao, Jingjin Dong, Duim Herman, H. Gert, ten Brink, Graeme R. Blake, Giuseppe Portale, Maria Antonietta Loi, Enhancing the crystallinity and perfecting the orientation of formamidinium tin iodide for highly efficient Sn-based perovskite solar cells, Nano Energy 60 (2019) 810–816.

[6] M.H. Kumar, S. Dharani, W.L. Leong, P.P. Boix, R.R. Prabhakar, T. Baikie, et al., Lead-free halide perovskite solar cells with high photocurrents realized through vacancy modulation, Adv. Mater. 26 (41) (2014) 7122–7127.

[7] A.G. Kontos, A. Kaltzoglou, E. Siranidi, D. Palles, G.K. Angeli, M.K. Arfanis, et al., Structural stability, vibrational properties, and photoluminescence in CsSnI3 perovskite upon the addition of SnF_2, Inorg. Chem. 56 (1) (2017) 84–91.

[8] F. Hao, C.C. Stoumpos, D.H. Cao, R.P.H. Chang, M.G. Kanatzidis, Lead-free solid-state organic–inorganic halide perovskite solar cells, Nat. Photon. 8 (2014) 489–494.

[9] A. Amat, E. Mosconi, E. Ronca, C. Quarti, P. Umari, M.K. Nazeeruddin, et al., Cation-induced band-gap tuning in organohalide perovskites: interplay of spin-orbit coupling and octahedra tilting, Nano Lett. 14 (6) (2014) 3608–3616.

[10] S.J. Lee, S.S. Shin, Y.C. Kim, D. Kim, T.K. Ahn, J.H. Noh, et al., Fabrication of efficient formamidinium tin iodide perovskite solar cells through SnF(2)-pyrazine complex, J. Am. Chem. Soc. 138 (12) (2016) 3974–3977.

[11] W. Liao, D. Zhao, Y. Yu, C.R. Grice, C. Wang, A.J. Cimaroli, et al., Lead-free inverted planar formamidinium tin triiodide perovskite solar cells achieving power conversion efficiencies up to 6.22, Adv. Mater. 28 (42) (2016) 9333–9340.

[12] W. Ke, C.C. Stoumpos, J.L. Logsdon, M.R. Wasielewski, Y. Yan, G. Fang, et al., TiO2-ZnS cascade electron transport layer for efficient formamidinium tin iodide perovskite solar cells, J. Am. Chem. Soc. 138 (45) (2016) 14998–15003.

[13] M. Ebner, F. Geldmacher, F. Marone, M. Stampanoni, V. Wood, Electrode materials: X-ray tomography of porous, transition metal oxide based lithium ion battery electrodes, Adv. Energy Mater. 3 (7) (2013) 845–850.

[14] T. Minemoto, M. Murata, Impact of work function of back contact of perovskite solar cells without hole transport material analyzed by device simulation, Curr. Appl. Phys. 14 (11) (2014) 1428–1433.

[15] T. Minemoto, M. Murata, Device modeling of perovskite solar cells based on structural similarity with thin film inorganic semiconductor solar cells, Appl. Phys. 116 (5) (2014), 054505.

[16] W. Abdelaziz, A. Shaker, M. Abouelatta-Ebrahim, A. Zekry, Abdelhalim, Possible efficiency boosting of non-fullerene acceptor solar cell using device simulation, Opt. Mater. 91 (2019) 239–245.

[17] D. Hui-Jing, W. Wei-Chao, Z. Jian-Zhuo, Device simulation of lead-free $CH_3NH_3SnI_3$ perovskite solar cells with high efficiency, Chin. Phys. B 25 (10) (2016), 108802.

[18] A. Niemegeers, M. Burgelman (Eds.), Numerical Modelling of AC-Characteristics of CdTe and CIS Solar Cells, Conference Record of the Twenty Fifth IEEE Photovoltaic Specialists Conference, 1996, pp. 13–17.

[19] M.D. Stamate, On the dielectric properties of dc magnetron TiO_2 thin films, Appl. Surf. Sci. 218 (1) (2003) 318–323.

[20] Evaluation of new materials for electron and hole transport layers in perovskite-based solar cells through SCAPS-1D simulations, in: S. Bansal, P. Aryal (Eds.), IEEE 43rd Photovoltaic Specialists Conference (PVSC) June, 2016, pp. 5–10.

[21] D. Poplavskyy, J. Nelson, Nondispersive hole transport in amorphous films of methoxy-spirofluorene-arylamine organic compound, Appl. Phys. 93 (1) (2003) 341–346.

[22] D. Liu, T.L. Kelly, Perovskite solar cells with a planar heterojunction structure prepared using room-temperature solution processing techniques, Nat. Photon. 8 (2013) 133.

[23] T.M. Koh, T. Krishnamoorthy, N. Yantara, C. Shi, W.L. Leong, P.P. Boix, et al., Formamidinium tin-based perovskite with low E_g for photovoltaic applications, J. Mater. Chem. 3 (29) (2015) 14996–15000.

[24] Z. Zhao, F. Gu, Y. Li, W. Sun, S. Ye, H. Rao, et al., Mixed-organic-cation tin iodide for lead-free perovskite solar cells with an efficiency of 8.12, Adv. Sci. 4 (11) (2017), 1700204.

[25] C. Kim, T.D. Huan, S. Krishnan, R. Ramprasad, A hybrid organic-inorganic perovskite dataset, Sci. Data 4 (2017), 170057.

[26] L.M. Herz, Charge-carrier mobilities in metal halide perovskites: fundamental mechanisms and limits, ACS Energy Lett. 2 (7) (2017) 1539–1548.

[27] S.J. Lee, S.S. Shin, J. Im, T.K. Ahn, J.H. Noh, N.J. Jeon, et al., Reducing carrier density in formamidinium tin perovskites and its beneficial effects on stability and efficiency of perovskite solar cells, ACS Energy Lett. 3 (1) (2018) 46–53.

[28] Hong-Hua Fang, Sampson Adjokatse, Shuyan Shao, Jacky Even, Maria Antonietta Loi, Long-lived hot-carrier light emission and large blue shift in formamidinium tin triiodide perovskites, Nat. Commun. 9 (1) (2018), 01685391.

[29] A. Zekry, Abdulhameed Yousef Al-Mazroo, A distributed spice-model of a solar cell, IEEE Trans. Electron. Dev. 43 (5) (1996) 691–700.

[30] V. Esteban, C. Juan Bernardo, J. Keony, V. Jaime, R. Daniel, J. Franklin, Numerical analysis to determine reliable one-diode model parameters for perovskite solar cells, Energies 11 (2018), 1996-1073.

[31] T.S. Sherkar, C. Momblona, L. Gil-Escrig, J. Ávila, M. Sessolo, H.J. Bolink, et al., Recombination in perovskite solar cells: significance of grain boundaries, interface traps, and defect ions, ACS Energy Lett. 2 (5) (2017) 1214–1222.
[32] A. Zekry, Electronic devices. https://www.researchgate.net/publication/236003006_Electronic_Devices, 1996.
[33] A. Zekry, A. Shaker, M. Salem, Chapter 1 - solar cells and arrays: principles, analysis, and design, Yahyaoui I, in: Advances in Renewable Energies and Power Technologies, Elsevier, 2018, pp. 3–56.
[34] Abdelhalim Zekry, Advanced solar cell materials and solar cells analytical modeling. https://www.researchgate.net/profile/Abdelhalim_Zekry/publication/320615297_Advanced_solar_cell_materials_and_solar_cells_analytical_modeling/data/59f08337458515bfd07bf883/white-paper-advanced-solar-cell-materials-and-solar-cells.pdf, 2017.
[35] Takashi Minemoto, Masashi Murata, Theoretical analysis on effect of band offsets in perovskite solar cells, Sol. Energy Mater. Sol. Cell. 133 (2015) 8–14.
[36] X. Gu, Y. Wang, T. Zhang, D. Liu, R. Zhang, P Zhang, J. Wu, Z. David Chen, L. Shibin, Enhanced electronic transport in Fe3+-doped TiO2 for high efficiency perovskite solar cells, J. Mater. Chem. 5 (41) (2017) 10754–10760.
[37] A. A, T. Leijtens, S. Pathak, J. Teuscher, R. Avolio, M. Errico, J. Kirkpatrik, J. Ball, P. Docampo, I. McPherson, H.J. Snaith, Lithium salts as “redox active” p-type dopants for organic semiconductors and their impact in solid-state dye-sensitized solar cells, Phys. Chem. C. 15 (7) (2013) 2572–2579.
[38] H. Syed Zulqarnain, A. Hafeez, W. Mingqing, A comprehensive device modelling of perovskite solar cell with inorganic copper iodide as hole transport material, Semicond. Sci. Technol. 33 (3) (2018), 035001.
[39] M. Salah, K. Hassan, M. Abouelatta, A. Shaker, A comparative study of different ETMs in perovskite solar cell with inorganic copper iodide as HTM, Optik 178 (2019) 958–963.